Acta Crystallographica Section D
Biological Crystallography
ISSN 0907-4449

Structure of relaxed-state human hemoglobin: insight into ligand uptake, transport and release

Joy D. Jenkins, Faik N. Musayev, Richmond Danso-Danquah, Donald J. Abraham and Martin K. Safo*

Department of Medicinal Chemistry, School of Pharmacy and Institute for Structural Biology and Drug Discovery, Virginia Commonwealth University, Richmond, VA 23219, USA

Correspondence e-mail: msafo@vcu.edu

Received 4 September 2008
Accepted 10 November 2008

PDB Reference: relaxed-state human hemoglobin, 3d17, r3d17sf.

Hemoglobin was one of the first protein structures to be determined by X-ray crystallography and served as a basis for the two-state MWC model for the mechanism of allosteric proteins. Since then, there has been an ongoing debate about whether Hb allostery involves the unliganded tense T state and the liganded relaxed R state or whether it involves the T state and an ensemble of liganded relaxed states. In fact, the former model is inconsistent with many functional observations, as well as the recent discoveries of several relaxed-state Hb structures such as RR2, R3 and R2. One school of thought has suggested the R2 state to be the physiologically relevant relaxed end state, with the R state mediating the T$\rightarrow$R2 transition. X-ray studies have been performed on human carbonmonoxy Hb at a resolution of 2.8 Å. The ensuing liganded quaternary structure is different from previously reported liganded Hb structures. The distal β-heme pocket is the largest when compared with other liganded Hb structures, partly owing to rotation of βHis63(E7) out of the distal pocket, creating a ligand channel to the solvent. The structure also shows unusually smaller α- and β-clefts. Results from this study taken in conjunction with previous findings suggest that multiple liganded Hb states with different quaternary structures may be involved in ligand uptake, stabilization, transport and release.

1. Introduction

The hemoglobin (Hb) tetramer is composed of two $\alpha\beta$ dimers ($\alpha1\beta1$–$\alpha2\beta2$) that are arranged around a twofold axis of symmetry, resulting in a large central water cavity. Ligand uptake and release by Hb has been described in terms of tense (T) and relaxed (R) state Hb. The T and R states have different quaternary structures which vary in the arrangement of the four-subunit tetramer. For instance, the allosteric transition between the two states results in rotation and translation of the $\alpha1\beta1$ dimer relative to the $\alpha2\beta2$ dimer by $\sim$14° and $\sim$1 Å, respectively (Baldwin & Chothia, 1979). The T and R states also differ in the conformation of the subunits, which is referred to as the tertiary structure. The structures of the T- and R-state Hbs were used to formulate the two-state MWC model for the mechanism of allosteric proteins (Monod *et al.*, 1965), which assumes that upon ligand binding the switch between these states involves the molecules as a whole without intermediate states. An alternative mechanism, known as the KNF model (Koshland *et al.*, 1966) and later refined by Perutz (Perutz, 1970, 1972, 1989; Perutz *et al.*, 1998), also assumes that upon ligand binding each subunit of the tetramer goes through a tertiary conformational change which

Table 1
Crystallographic data and refinement statistics.

Values in parentheses are for the outermost resolution bin.

Data collection	
Space group	$P4_12_12$
Unit-cell parameters (Å)	$a = b = 87.3$, $c = 174.5$
Resolution (Å)	39.0–2.8 (2.90–2.80)
No. of measurements	57804 (5780)
Unique reflections	16653 (1633)
$I/\sigma(I)$	7.8 (3.7)
Completeness (%)	95.8 (95.9)
$R_{\rm merge}$† (%)	12.8 (35.2)
Refinement	
Resolution limit (Å)	19.9–2.8 (2.97–2.80)
σ cutoff on F	2.5
R factor (%)	23.2 (35.0)
$R_{\rm free}$‡ (%)	29.7 (37.7)
No. of reflections	16148 (2590)
Completeness (%)	93.5 (92.0)
R.m.s.d. from standard geometry	
Bond lengths (Å)	0.01
Bond angles (°)	1.90
Dihedral angles (°)	
Ramachandran plot, residues in (%)	
Most favored regions	85.5
Additionally allowed regions	14.5
Average B factors (Å^2)	
Protein alone	40.65
Heme	40.55
Water	23.68

† $R_{\rm merge} = \sum_{hkl}\sum_i |I_i(hkl) - \langle I(hkl)\rangle| / \sum_{hkl}\sum_i I_i(hkl)$. ‡ 5% of reflections were excluded from refinement and used for the calculation of $R_{\rm free}$.

is then transmitted to another subunit through direct communication, leading to sequential changes in the affinity for ligand. Perutz suggested that the low oxygen affinity of the T-state is the consequence of strain at the F helix that causes the proximal histidine (F8) to move the Fe atom out of the plane of the porphyrin ring, as well as of steric hindrance to ligand binding at the β-heme by the distal residues His63(E7) and Val67(E11) (Perutz, 1970, 1972, 1989; Perutz *et al.*, 1998). This led to the proposition that ligand must first bind to the less sterically hindered α-heme to relieve the strain at the αF helix, causing the αFG corner to move toward the β-subunit of the opposite dimer (Perutz, 1970, 1972, 1989; Perutz *et al.*, 1998). The resulting intersubunit communication is believed to decrease the strain at the β-subunit proximal histidine as well as relieve the steric hindrance at the β-heme, with a concomitant enhancement of ligand binding (Perutz, 1970, 1972, 1989; Perutz *et al.*, 1998). Binding of ligand at the β-heme is also suggested to lead to intersubunit communication and facilitate an increased uptake of oxygen at the α-heme (Perutz, 1970, 1972, 1989; Perutz *et al.*, 1998). The assumption that Hb exists as two end states without any intermediate states has been challenged over the years.

Several studies have now shown that the allosteric transition between the tense and relaxed states is mediated by multiliganded Hb states, with each form exhibiting variable oxygen affinities (Minton & Imai, 1974; Sawicki & Gibson, 1976; Yonetani *et al.*, 2002; Marden *et al.*, 1988; Lee *et al.*, 1988; Jayaraman & Spiro, 1995; Perrella *et al.*, 1990; Perrella & Di Cera, 1998). Various authors have correlated this observation with conformational variations of the liganded states, which were found to be dependent on changes in protons, chloride ions, 2,3-diphosphoglycerate (2,3-DPG), pH *etc.* (Minton & Imai, 1974; Sawicki & Gibson, 1976). The functional observations that liganded Hb exists as multiple states each with a distinct conformation seems to be consistent with the recent discoveries of several liganded Hb structures with different relaxed conformations, including the R2, RR2 and R3 states (Silva *et al.*, 1992; Smith *et al.*, 1991; Mueser *et al.*, 2000; Safo & Abraham, 2003, 2005; Safo *et al.*, 2004). Unless noted otherwise, the term 'relaxed state' is used here to refer to all the different liganded Hb structures. It has been suggested that the R2 state may be the physiologically relevant relaxed end state instead of the previously thought R state and that the R and RR2 states are intermediates during the T→R2 transition (Safo & Abraham, 2005; Janin & Wodak, 1993; Doyle *et al.*, 1992; Srinivasan & Rose, 1994; Schumacher *et al.*, 1997). The R3 state has also been suggested to be a relaxed end state (Safo & Abraham, 2005). The functional or physiological significance of the R3 state has not presently been elucidated; however, this structure shows the most relaxed geometrical features of known liganded Hb structures (Safo & Abraham, 2005).

In this work, we report a CO-bound Hb quaternary structure. Comparison of this structure with the crystal structures of Hb in the T, R, RR2, R2 and R3 states shows it to have unique differences and sheds light on the possible functional roles of R-, RR2-, R2- and R3-state Hbs.

2. Experimental procedures

2.1. Crystallization, data collection and data processing

Hemoglobin was deoxygenated (deoxyHb) under vacuum and then fully saturated with carbon monoxide to generate the CO-ligated form. A room-temperature crystallization experiment was carried out with a solution of 30–50 mg ml^{-1} protein, 3.2 *M* sodium/potassium phosphate pH 6.4 and two drops of toluene in 10 ml vacutainer tubes as described previously (Safo & Abraham, 2003, 2005). Three different crystal forms (rectangular prisms, octahedra and thin needles) were isolated from the same crystallization tube. Prior to use in diffraction, the crystals were washed in a cryoprotectant solution containing 50 µl mother liquor and 10–12 µl glycerol and then flash-frozen. X-ray diffraction data were collected at 100 K using a Molecular Structure Corporation (MSC) X-Stream Cryogenic Cooler System (MSC, The Woodlands, Texas, USA), an R-AXIS IV^{++} image-plate detector and a MicroMax-007 microfocus rotating-anode X-ray generator operating at 20 kV and 40 mA. The needle-shaped, rectangular prismatic and octahedral crystals diffracted to 2.8, 2.1 and 2.0 Å resolution, respectively. The data were processed with the MSC *d*TREK* software and the *CCP*4 suite of programs (Collaborative Computational Project, Number 4, 1994). Structure refinements were performed with *CNS* (Brünger *et al.*, 1998). Model building and correction were carried out using *TOM* (Cambillau & Horjales, 1987). The X-ray data from a needle-shaped crystal are summarized in Table 1. The

program *LSQKAB* (Collaborative Computational Project, Number 4, 1994) and the stand-alone program *ALIGN* were used for structure comparison (Cohen, 1997).

2.2. Structure determination and refinement

The Matthews coefficient of 2.6 Å^3 Da^{-1} and water content of 52% were consistent with the presence of two dimers (one tetramer) per asymmetric unit. The structure was determined from the needle-shaped crystal by the *AMoRe* molecular-replacement method (Navaza, 1994) using the $\alpha1\beta1$–$\alpha2\beta2$ coordinates of the R-state Hb structure (PDB code 1ljw; Safo *et al.*, 2002) as a search model. Note that the crystallographic asymmetric unit of 1ljw contains a dimer; the tetramer model used for the molecular-replacement search was generated using the appropriate crystal symmetry. The translation function in space group $P4_12_12$ gave a solution with a tetramer ($\alpha1\beta1$–$\alpha2\beta2$) in the asymmetric unit with a final correlation coefficient of 43.3 and an *R* factor of 45.5% at 4 Å resolution. The solution model was then subjected to rigid-body refinement followed by conjugate-gradient minimization and then simulated annealing, resulting in an *R* factor of 28.96% and an $R_{\rm free}$ of 37.87%. At this stage, a noncrystallographic symmetry (NCS) restraint was applied to all atoms and the model was subjected to further refinement. It became apparent that several regions of the molecules (such as the residues at the interdimer interface) were different between the $\alpha1\beta2$ and the $\alpha2\beta1$ dimers and the NCS restraints at these positions were released. The electron-density maps showed ligation of the $\beta1$-heme, $\beta2$-heme and $\alpha1$-heme irons, which were fitted with CO. Several more alternate rounds of refinement (with an NCS restraint weight of 30 applied to ∼60% of the model) and the addition of 80 water molecules, one toluene molecule and three phosphate ions with intermittent manual model corrections brought the final *R* factor to 23.2% and the $R_{\rm free}$ to 29.7% at 2.8 Å resolution using data above 2.5σ cutoff on *F*.

The octahedral crystal belonged to space group $P4_12_12$, with unit-cell parameters $a = b = 53.6$, $c = 193.2$ Å, while the rectangular prismatic crystal belonged to space group $P4_122$, with unit-cell parameters $a = b = 63.3$, $c = 174.7$ Å. The two structures were only partially refined to *R* factor/$R_{\rm free}$ values of 23.2%/26.8% (2.0 Å resolution) and 22.6%/25.3% (2.1 Å resolution), respectively, using the respective isomorphous R- and R3-state structures as models.

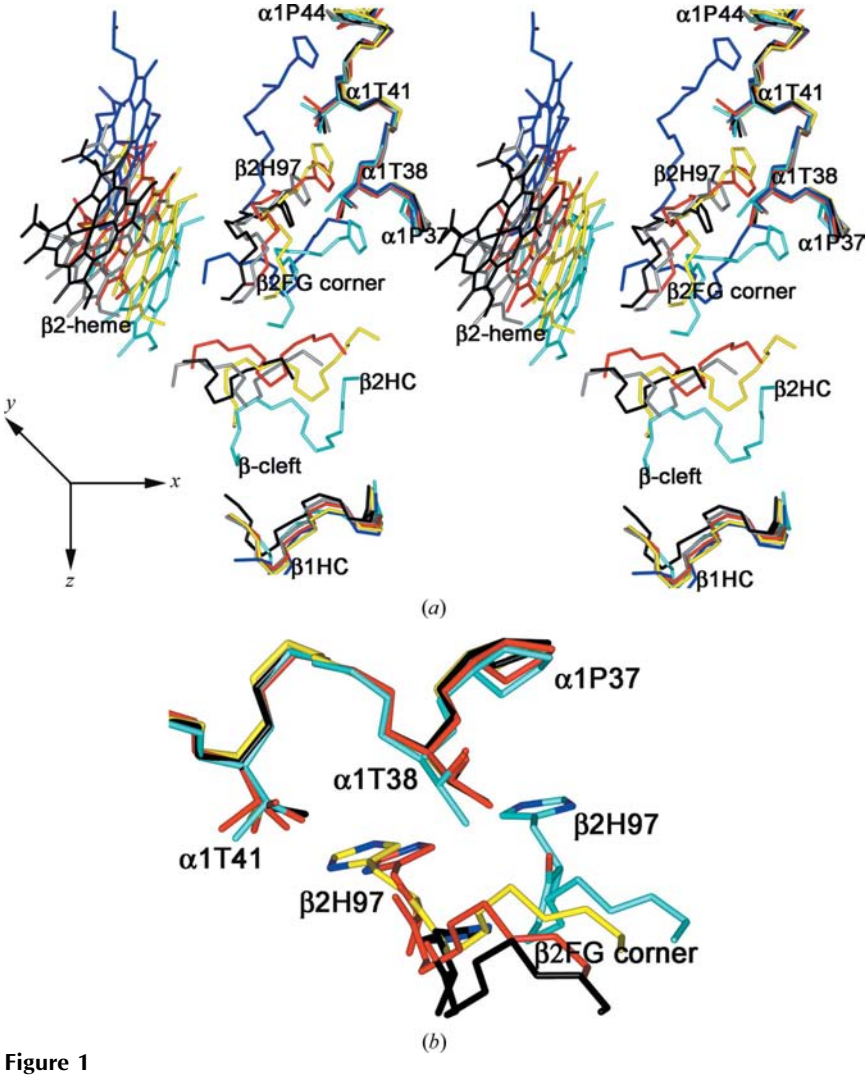

Figure 1
(*a*) A stereoview of the $\alpha1\beta2$ dimer interface, the $\beta2$-heme and the β-cleft after COHbA (yellow) and the T state (blue), R state (red), R3 state (cyan), RR2 state (grey) and R2 state (black) were superimposed with their $\alpha1\beta1$ dimers. The allosteric transition from the T state to the relaxed states has moved the $\beta2$ subunit towards the central water cavity (the *z*-axis direction) relative to both the $\alpha1$ subunit and the $\beta1$ subunit. The figure also reveals the unusual structural characteristics of COHbA. Part of the $\beta2$FG corner (residues 96 and 97) of COHbA is closer to the R state, while the other part (residues 98–103) is located between the R and R3 states. The position of the $\beta2$-heme and the size of the β-cleft of COHbA are intermediate between those of the R and R3 states. (*b*) A zoomed monoview of the $\alpha1\beta2$ dimer interface (orientated at 90° from Fig. 1*a*), showing the relative position of $\beta2$His97 in COHbA (yellow) and the R state (red), R3 state (cyan) and R2 state (black). The T state and RR2 state are not shown for clarity. The figures were generated using *INSIGHT*II (Molecular Simulations Inc., San Diego, California, USA).

3. Results

3.1. Crystallization experiment and structural analysis

The crystallization experiment resulted in a thin needle-shaped crystal and the ensuing structure had one Hb tetramer in the asymmetric unit. In addition, two further crystal forms, octahedra and rectangular prisms, each with a Hb dimer ($\alpha1\beta1$) in the asymmetric unit, were obtained from the same crystallization tube. These two crystals were isomorphous with previously deter-

mined R- and R3-state structures, respectively. The latter two structures were not refined to conclusion since they showed no significant tertiary or quaternary structural differences from the published isomorphous structures. The needle-shaped crystal belonged to space group $P4_12_12$, with unit-cell parameters $a = b = 87.3$, $c = 174.5$ Å, while the rectangular prismatic R3-state crystal belonged to space group $P4_122$, with unit-cell parameters $a = b = 63.3$, $c = 174.7$ Å. The c axis of the needle-shaped crystal is identical to that of the R3-state crystal and the a and b axes of the former are similar to the ab diagonal of the latter. A native Patterson map of the needle-shaped crystal shows a large peak (∼31% of the origin) at $\frac{1}{2}, \frac{1}{2}, 0$. This pseudo-translational symmetry relates one crystal to another.

The needle-shaped crystal showed difference densities at the β2-heme, β1-heme and α1-heme irons, which we deduced to be bound by CO molecules. However, we cannot rule out a mixture of water and CO. On the other hand, the $F_o - F_c$ and $2F_o - F_c$ maps contoured at very low levels (2.2σ and 0.7σ, respectively) showed no discernable ligand density at the α2-heme and we surmise that this heme may be in the unliganded metHb state.

3.2. Structural comparison

Comparison of the structure reported here obtained from the needle-shaped crystal (COHbA) with other Hb structures, including those of the T state (PDB entry 2hhb; Fermi *et al.*, 1984), R state (1aj9; Vásquez *et al.*, 1998), RR2 state (1mko; Safo & Abraham, 2005), R2 state (1bbb; Silva *et al.*, 1992) and R3 state (1yzi; Safo & Abraham, 2005), by superposition of their $\alpha1\beta1$ dimers (C^α residues) reveals similar overall tertiary conformations (r.m.s.d.s of 0.3–0.6 Å). Superposition with the T state resulted in an r.m.s.d. of 0.9 Å. Nevertheless, significant tertiary structural differences occur at the heme pocket and/or the interdimer interface involving the E helix, F helix and FG corner residues. The quaternary structural differences between the Hb structures as noted by superposition of the complete $\alpha1\beta1$–$\alpha2\beta2$ tetramers showed the conformation of COHbA to be closest to the R and R3 states, with an r.s.m.d. of 1.1 Å; the r.m.s.d. was 1.6 Å with the RR2 state, 2.0 Å with the R2 state and 2.3 Å with the T state. Other quaternary differences as quantified by screw-rotation angle/translation of the nonsuperimposed $\alpha2\beta2$ Hb dimers after superimposition of the $\alpha1\beta1$ dimers of the various Hb structures (not shown) are also consistent with COHbA having a quaternary structure intermediate between those of the R and R3 state.

Fig. 1 captures some of the quaternary differences between the structures after superimposing the $\alpha1\beta1$ dimers. In all instances, the allosteric switch from the T state to the relaxed states (involving rotation/translation of $\alpha2\beta2$ relative to $\alpha1\beta1$) has resulted in a sliding motion between the $\beta2$ subunit and the opposite $\alpha1$ subunit. Of particular interest is the $\beta2$ FG

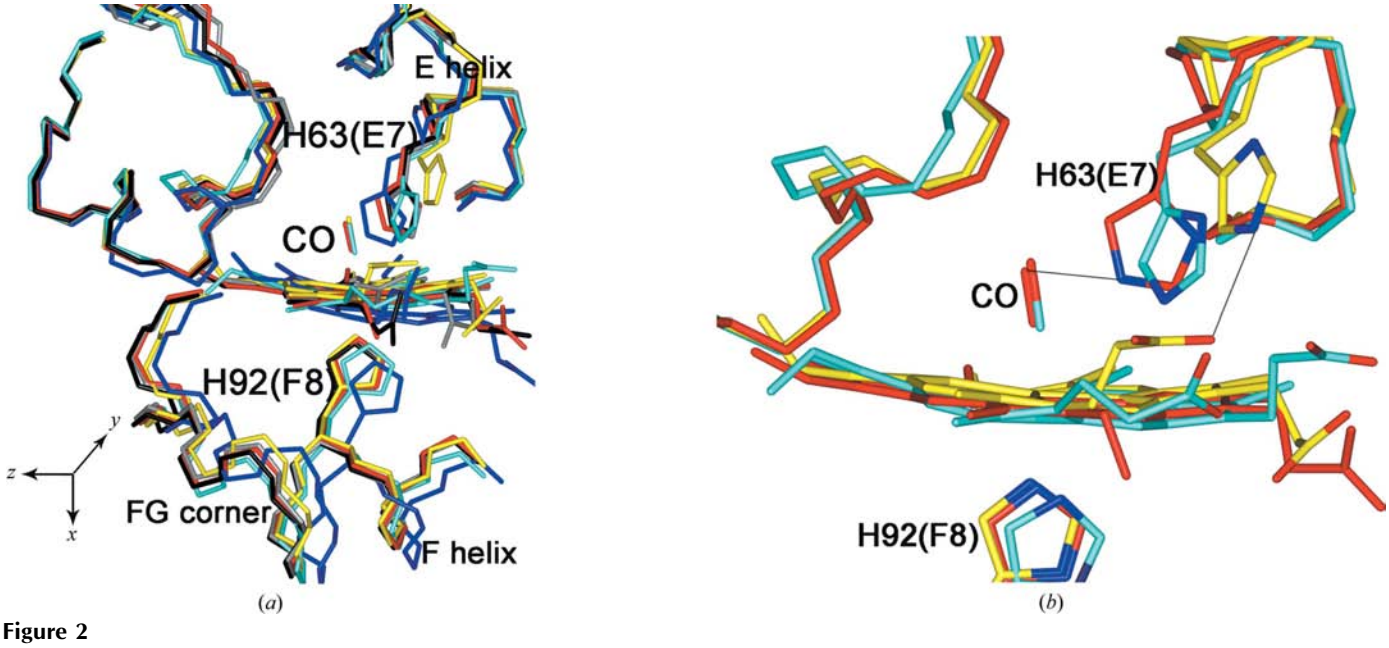

Figure 2
(*a*) Tertiary structural comparison of the β1-heme of COHbA (yellow) and of the T state (blue), R state (red), R3 state (cyan), RR2 state (grey) and R2 state (black). The structures were superimposed with their β1 subunits. Subtle movement of the E helices from the ligand position has led to a significant size increase in the distal β-heme pocket in the relaxed-state structures compared with the T-state structure. There is a rotation of βHis63(E7) out of the distal pocket in the COHbA, creating a ligand channel to the bulk solvent, while in the R, RR2 and R2 states βHis63 is still located in the distal pocket. The βHis63 of the R3 state is in an intermediate position between those of COHbA and the R state. In the T state, βHis63 is very close to the ligand position and would undoubtedly lead to steric interference with an incoming or a bound ligand. The βFG corners of the relaxed states have also shifted toward the central water cavity (the z-axis direction) from the T-state position. (*b*) An enlarged view of the distal β1-heme pockets of COHbA (yellow), the R state (red) and the R3 state (cyan). The RR2, R2 and T states are not shown for clarity. Note that in the R state the imidazole N atom makes a hydrogen-bond interaction with the CO. A similar hydrogen-bond interaction is also observed in the R2 and RR2 states because their βHis63 residues are located in similar positions to that of the R state. Rotation of the βHis63 in COHbA has moved this residue more than 6 Å from the CO position to make a hydrogen-bond interaction with the heme propionate. Rotation of βHis63 in the R3 state has moved this residue about 4 Å from the CO position. The figures were generated with *INSIGHT*II (Molecular Simulations Inc., San Diego, California, USA).

corner (residues 96–103), which has moved relative to the α1C helix (residues 36–44) at the $\alpha1\beta2$ dimer interface toward the central water cavity (the z-axis direction in Fig. 1*a*). Overall, the quaternary movement has led to a significant reduction in the size of the central water cavity in the liganded Hbs compared with the T state, with that of the R3 state being the smallest. COHbA also shows a smaller central water-cavity size compared with the R-, RR2- and R2-state structures. The reduction in the size of the water cavity is believed to contribute to intersubunit communication, forming one of the bases of Perutz's stereochemical theory (Perutz, 1970, 1972, 1989; Perutz *et al.*, 1998).

The allosteric sliding motion discussed above has resulted in the FG corner residue β2His97, which sits between α1Pro44 and α1Thr41 in the T state, to move by a turn into another groove formed by α1Thr41 and α1Thr38 in the R state, in which β2His97 makes a hydrogen-bond interaction with α1Thr38 (Fig. 1*b*). The observation that β2His97 jumps from one groove in the T state to another in the R state led to the suggestion that only two relative positions of the α1 and β2 subunits are stable, forming the structural basis of the two-state allosteric model (Perutz, 1970, 1972, 1989; Perutz *et al.*, 1998). The discoveries of the RR2 and R2 states show that the β2FG corner can rotate further in a perpendicular fashion from the R-state position, resulting in the disengagement of the hydrogen-bond interaction between β2His97 and α1Thr38 found in the R state. In a remarkable fashion, the β2FG corner of the R3 state has moved even closer towards the central water cavity from the R-state position, bringing β2His97 to pack between α1Thr38 and α1Pro37 (Fig. 1*b*). In COHbA, β2His97 has shifted slightly toward the T-state position compared with that of the R state; however, the rest of the β2FG corner (residues 98–103) is located in between the R- and R3-state positions (Fig. 1*b*). The new position of β2His97 in COHbA suggests a possible hydrogen-bond interaction between β2His97 and α1Thr41 (Fig. 1*b*). Interestingly, at the symmetry-related $\alpha2\beta1$ interface in COHbA, β1His97 is positioned at almost the same location as that of the R state (not shown).

The movement of the β subunit relative to the opposite α subunit has also resulted in some remarkable quaternary structural features at both the β-cleft and the α-cleft, which define the two entry points into the central water cavity. In the R3 state, the β2 subunit (H helix, HC segment, NA segment and F helix) has moved toward the β1 subunit counterpart to completely block the β-cleft, while the corresponding β-cleft in COHbA is also significantly reduced compared with the R, R2 and RR2 states (Fig. 1*a*). The T state has the largest β-cleft. A similar trend is observed for the α-cleft, but on a significantly smaller scale (not shown).

3.3. The heme environment

In the β subunits, the stereochemical parameters between the proximal histidine βHis92(F8) and the heme are similar in the liganded Hb structures, but different from the T-state structure. However, ligand uptake in the relaxed Hbs results in significant tertiary conformational differences at the FG corners, which are displaced toward the dimer interface (the direction of the z axis in Fig. 2*a*). We also observe significant differences between the distal histidine βHis63 and the heme in all the structures (Fig. 2*a*). In the T state, the distance between the βHis63 imidazole and a putative bound ligand is about 1.9 Å. Clearly, such a close contact would result in unfavorable ligand binding and partly explains why the β-heme of T-state Hb has been proposed to have a lower affinity for oxygen (Perutz, 1970, 1972, 1989; Perutz *et al.*, 1998). In the relaxed states, the E helix (in particular the side chains of βHis63 and βVal67) is displaced from the ligand position, creating a larger distal pocket that should lead to

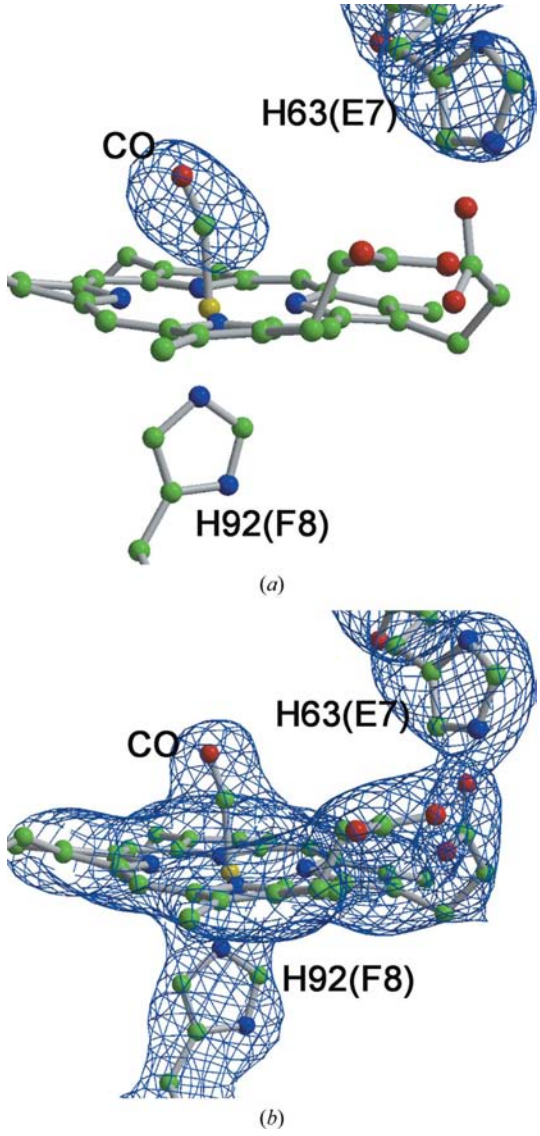

Figure 3
(*a*) An OMIT map at the β2-heme, which was calculated by omitting CO and βHis63 during simulated annealing. The map was contoured at the 1.0σ level and then superimposed with the final refined model. (*b*) A final $2F_o - F_c$ map of the β2-heme contoured at the 1.0σ level, showing a possible strong hydrogen-bond/salt-bridge interaction between the heme propionate and βHis63. The map is superimposed with the final refined model. The figures were drawn using *BOBSCRIPT* (Esnouf, 1997) and *RASTER3D* (Merritt & Murphy, 1994).

decreased steric hindrance between the incoming or bound ligand (Figs. 2*a* and 2*b*). In the R, RR2 and R2 states, the displaced βHis63 imidazole, although still located in the distal heme pocket, makes a ~3 Å hydrogen-bond interaction to the oxygen of the O_2 or CO ligand (Fig. 2*b*). Remarkably, in COHbA, besides the subtle movement of the E helix from the distal pocket, there is an ~90° rotation of βHis63 at the $C^{\alpha}-C^{\beta}$ bond that places the imidazole out of the distal pocket by about 3 Å from the R-state position (Figs. 2*a* and 2*b*). The closest distance between the βHis63 imidazole and CO is 6.6 Å. It seems that the rotation of βHis63 has resulted in an interaction between the imidazole NE2 and the β-heme propionate (Figs. 2*b*, 3*a* and 3*b*). The pK_a of βHis63 has been reported to be 5.8 (Schweitzer-Stenner *et al.*, 1986) and the histidine should therefore exist in an appreciably protonated form at the pH of 6.4 used to obtain the crystals. Thus, the interaction between βHis63 and the heme propionate is probably a salt bridge, which should be able to stabilize this conformation. The ND1 atom of the imidazole also makes a possible hydrogen-bond contact with the carboxyl group of Glu90 of a symmetry-related molecule (not shown). At the β1-heme, the imidazole of β1His63 has similarly rotated away from the distal pocket to make a hydrogen-bond contact with the heme propionate. There is no crystal contact involving β1His63 and this is manifested in β1His63 showing a weaker side-chain density compared with that of β2His63; this is also reflected in their *B* factors. As a consequence of the βHis63 rotation, a larger distal pocket as well as a ligand channel to the bulk solvent has been created in the COHbA structure compared with the other liganded Hb structures. The βHis63 position in the R3-state structure presents an interesting case in which the imidazole has only rotated about 1 Å from the R-state location and clearly depicts an intermediate open position (Figs. 2*a* and 2*b*). The closest distance between the βHis63 imidazole and the bound CO atom is ~4 Å, compared with the 3 and 6.6 Å observed in the R state and COHbA, respectively.

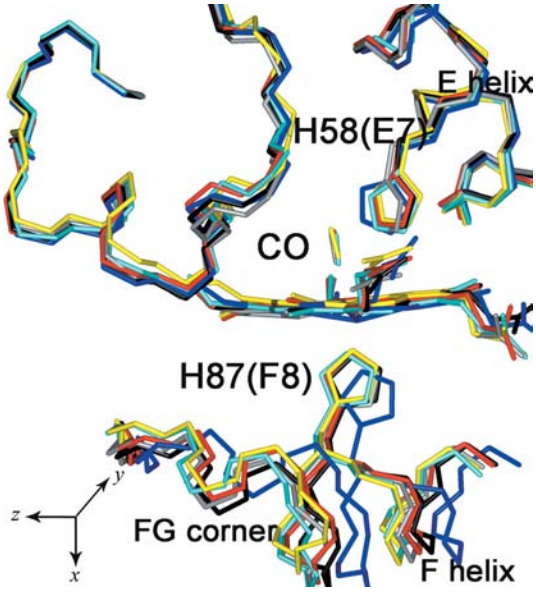

Figure 4
Tertiary structural comparison of the α1-heme of COHbA (yellow) and of the T state (blue), R state (red), R3 state (cyan), RR2 state (grey) and R2 state (black). The structures were superimposed with their α1 subunits. The αFG corners of the relaxed states have moved toward the central water cavity from the T-state position, with the R3 state showing the greatest shift, followed by COHbA and then the R state, with the R2 state showing the least shift. His58(E7) of the relaxed states has shifted ~0.7 Å from the T-state position and away from the ligand position, with a concomitant distal-pocket size increase in the liganded structures. This figure was generated with *INSIGHT*II.

At the α-hemes, the stereochemical geometry between the proximal histidine and the heme, as well as between the distal histidine and the heme, are very similar in the liganded Hbs, but differ significantly from those of the T state (Fig. 4). Like the βFG corner, but even more pronounced, the αFG corners of the liganded structures have moved toward the dimer interface and central water cavity (in the direction of the *z* axis in Fig. 4). However, the E helices of the liganded Hbs do not seem to differ significantly from the T-state position, with the exception of the side chain of the distal histidine αHis58(E7), which is displaced from the ligand position. As a result, the putative distance between αHis58 and CO is ~2.6 Å in the T-state structure, compared with 3.2–3.4 Å in the COHbA, R-, R2-, R3- and RR2-state structures.

4. Discussion

This paper reports a new relaxed-state Hb structure, COHbA, with three of the four hemes ligated. Other relaxed-state Hb structures have previously been reported in the literature; notable structures are the R, RR2, R2 and R3 states, with the latter showing the most relaxed structural features (Safo & Abraham, 2005). Crystals of COHbA appeared in conjunction with R- and R3-state Hb crystals. We note that previous studies have also resulted in a mixture of R-, RR2- and R3-state Hb crystals, while others have also isolated a mixture of R- and R2-state or RR2-state-like Hb crystals (Mueser *et al.*, 2000; Safo & Abraham, 2005; Biswal & Vijayan, 2001; Sankaranarayanan *et al.*, 2005). Moreover, an NMR study at near-physiological conditions of pH and ionic strength showed that liganded Hb exists as a mixture of R-state, R2-state and RR2-state-like Hbs in solution (Lukin *et al.*, 2003). The question we ask is whether all these liganded states are physiologically relevant and if so what are their specific roles in Hb function?

Our structural analysis shows that the central water cavity, including the α- and β-clefts, is significantly different in the various Hb structures, partly owing to variations in the sliding motion of the βFG corner relative to the αC helix of the opposite dimer. The T state, which has the largest α- and β-clefts, has been suggested to facilitate the flow of chloride ions to neutralize positive charges in the central water cavity (chloride-dependent alkaline Bohr effect), as well as to bind with high affinity to 2,3-DPG at the β-cleft. The effect is to stabilize and decrease the oxygen affinity of the T-state, which is consistent with the physiological function of this Hb state. The R3 state, which has the smallest cleft among the liganded structures, has also been suggested to impede the flow of

negative ions, as well as to completely preclude binding of 2,3-DPG (Safo & Abraham, 2005). COHbA and the R, RR2 and R2 states, which have varying intermediate α- and β-cleft sizes, may decrease the flow of chloride ions to varying degrees and may also bind 2,3-DPG, albeit more weakly, as has been suggested by several studies (Yonetani *et al.*, 2002; Safo & Abraham, 2005; Gupta *et al.*, 1979; Safo *et al.*, 2002). In fact, a phosphate molecule is observed to be bound at the 2,3-DPG-binding site in the COHbA, RR2-state and R-state structures. In effect, the different liganded Hbs may exhibit different affinities for oxygen depending on the size of the central water cavity (the closeness of the opposite dimers), the size of the α- and β-clefts and perhaps the binding of heterotrophic molecules to the clefts that should stabilize or destabilize a particular relaxed-state conformation. Consistently, a study by Minton & Imai (1974) showed a correlation between variable oxygen affinity and conformational variations of liganded states, which were found to be dependent in changes in protons, chloride ions, 2,3-DPG *etc.*

As a consequence of the βHis63 rotation in COHbA, a larger distal β-heme pocket and a ligand channel to the bulk solvent have been created in this structure compared with the other liganded Hb structures and should facilitate ligand access to the β-hemes. Perutz previously predicted such a rotation of the βHis63 imidazole out of the distal pocket for the access of ligand (Perutz, 1989). Various studies with myoglobin and other non-mammalian Hbs have also observed such a ligand channel (Yang & Phillips, 1996; Tian *et al.*, 1993; Vallone *et al.*, 2004; Geibel *et al.*, 1975; Cannon *et al.*, 1976; Traylor *et al.*, 1983; Akiyama *et al.*, 1994). To the best of our knowledge, the present study provides the first direct structural evidence for an opened ligand channel in mammalian Hb. It seems that the dynamics of βHis63 are a consequence of tertiary changes in the E helix and are possibly also pH-dependent. Relatively low pH should stabilize the open ligand-channel conformation as observed in COHbA and to some extent in the R3 state, while high pH should favor closure of the channel as observed in the R, RR2 and R2 states. Indeed, R- and R3-state crystals predominate at high pH (>6.5) and low pH (<6.5), respectively (Safo & Abraham, 2005). R2-state crystals were originally reported to occur at the low pH of 5.8 (Silva *et al.*, 1992), but we and others have shown that these crystals can easily be obtained at higher pH values (>6.5; Safo *et al.*, 2004; Biswal & Vijayan, 2001; Sankaranarayanan *et al.*, 2005). pH-dependent movement of the distal βHis63 has also been reported in several studies with myoglobin and non-mammalian hemoglobin (Tian *et al.*, 1993; Vallone *et al.*, 2004; Geibel *et al.*, 1975; Cannon *et al.*, 1976; Traylor *et al.*, 1983; Akiyama *et al.*, 1994). For example, in murine neuroglobin the βHis63 imidazole is found to make a hydrogen-bond interaction with CO as described above for the R-state Hb at neutral or high pH, while at low pH the imidazole is observed to be swung out of the distal pocket as described above for COHbA (Vallone *et al.*, 2004). The rate constant for ligand binding to myoglobin has also been reported to increase with a decrease in pH (Geibel *et al.*, 1975; Cannon *et al.*, 1976; Traylor *et al.*, 1983). Consistently, the crystal structures of myoglobin at pH 4, 5 and 6 show varying conformation, with the structure at pH 4 showing rotation of β63His out of the distal pocket (Yang & Phillips, 1996).

Unlike the β-heme, there is no evidence to suggest that ligand access at the α-heme involves a ligand channel created by rotation of the distal βHis58 as described above for the β-heme. Rather, as proposed in an alternate mechanism, ligand may diffuse into the α-heme through several hydrophobic pathways between the B, G and H helices of the heme cavity (Elber & Karplus, 1990).

In the R, RR2, R3 and R2 states all four hemes are ligated; however, in COHbA only the two β-hemes and the α1-heme have ligand bound, while the α2-heme is most likely to be in an unliganded metHb form. We propose that COHbA, with its fully opened distal β-heme ligand channel, captures a relaxed Hb conformation during ligand uptake, while the R3 state may capture on a molecular level the fully ligated relaxed Hb conformation in the process of closing the ligand channel at the β-heme. Note that in the R3 state the two βHis63 residues are in an intermediate open position and the CO at the β-hemes is loosely bound. Interestingly, the COHbA (tetramer in the asymmetric unit) and R3-state (dimer in the asymmetric unit) crystals are closely related by a near-perfect translational symmetry, which is consistent with the idea that the two Hb states could easily interconvert. The binding of three ligands along with the significant structural differences found at the dimer interfaces of $\alpha1\beta2$ compared with those of $\alpha2\beta1$ could explain the break in symmetry. If our supposition is correct, then it seems that the structural changes in the two symmetry-related Hb dimer interfaces ($\alpha1\beta2$ and $\alpha2\beta1$) do not necessarily occur at the same time during the allosteric transition and are tied to differences in the heme ligation, which is consistent with Perutz's stereochemical mechanism for sequential ligand binding (Perutz, 1970, 1972, 1989; Perutz *et al.*, 1998). Subsequent ligand stabilization in the R3 state should occur by further movement of the E helix towards the ligand position where βHis63 can make a hydrogen-bond interaction with the heme ligand. This process represents a shift of the R3-state conformation to the liganded states of the R, RR2 and R2 states, where the latter three structures show more tightly packed distal pockets as well as closed ligand channels. Elimination of exogenous ligand from the hemes to the tissues may also occur in the reverse order, which also involves a rotation of the distal βHis63 out of the distal β-heme pocket. Based on these analyses, it is very tempting to speculate that COHbA and/or the R3 state represent Hb conformations that are actively involved in both ligand uptake and/or release, while the role of the R2 state and/or R state and/or RR2 state is to act as temporary storage of bound ligand for transport. Our hypothesis of the R, RR2 and R2 states serving as temporary storage of bound ligand is bolstered by the argument that the strong hydrogen-bond interaction between the heme-bound ligand and βHis63, as well as the packed distal pocket, do not support the idea that the ligand can bind or be released efficiently from these relaxed-state Hbs. A correlation between pH, ligand binding/release and quaternary form can also be made. At relatively

high pH the bound oxygen is in a storage mode in the R2- or RR2- or R-state conformation, while at relatively low pH during oxygen uptake or release the COHbA and/or R3 state predominate. Consistently, lower pH arising from proton release by metabolic products such as lactic and carbonic acids is known to facilitate the release of oxygen to the tissues from Hb. Also, studies using trout IV, carp and spot Hbs indicate large increases in both the rate of ligand dissociation and association as the pH is lowered (Brunori *et al.*, 1974; Noble *et al.*, 1970; Bonaventura *et al.*, 1976). Finally, transition from the liganded state to the T state is known to be faster at the low pH of 5.8 than at neutral pH (Kaminaka & Kitagawa, 1992).

5. Conclusion

The data presented here strongly suggest that the different liganded Hb states observed in various studies may be an ensemble of ligated species, such as the R, R2, RR2, R3 states and COHbA, each of which has its own distinct quaternary and relaxed structural features and as a result its own affinity for oxygen. These different structures reflect multiple allosteric effects with distinct functions that are the outcome of oxygen tension, ionic strength, pH, chloride, 2,3-DPG, temperature and other heterotrophic effects. It is quite obvious that Hb allostery is more complicated than the two-state model or its modification thereof that suggests that ligand binding goes through a tertiary conformational change without a quaternary change. It is only when multi-liganded states are invoked that we can begin to paint a complete picture of how Hb functions.

References

Akiyama, K., Fukuda, M., Kobayashi, N., Matsuoka, A. & Shikama, K. (1994). *Biochim. Biophys. Acta*, **1208**, 306–309.

Baldwin, J. & Chothia, C. (1979). *J. Mol. Biol.* **129**, 175–220.

Biswal, B. K. & Vijayan, M. (2001). *Curr. Sci.* **81**, 1100–1105.

Bonaventura, J., Bonaventura, C., Sullivan, B., Ferruzzi, G., McCurdy, P. R., Fox, J. & Moo-Penn, W. F. (1976). *J. Biol. Chem.* **251**, 7563–7571.

Brünger, A. T., Adams, P. D., Clore, G. M., DeLano, W. L., Gros, P., Grosse-Kunstleve, R. W., Jiang, J.-S., Kuszewski, J., Nilges, M., Pannu, N. S., Read, R. J., Rice, L. M., Simonson, T. & Warren, G. L. (1998). *Acta Cryst.* D**54**, 905–921.

Brunori, M., Falcioni, G. & Rotilio, G. (1974). *Proc. Natl Acad. Sci. USA*, **71**, 2470–2472.

Cambillau, C. & Horjales, E. (1987). *J. Mol. Graph.* **5**, 174–177.

Cannon, J., Geibel, J., Whipple, M. & Traylor, T. G. (1976). *J. Am. Chem. Soc.* **98**, 3395–3396.

Cohen, G. E. (1997). *J. Appl. Cryst.* **30**, 1160–1161.

Collaborative Computational Project, Number 4 (1994). *Acta Cryst.* D**50**, 760–763.

Doyle, M. L., Lew, G., Turner, G. J., Rucknagel, D. & Ackers, G. K. (1992). *Proteins*, **14**, 351–362.

Elber, R. & Karplus, M. (1990). *J. Am. Chem. Soc.* **112**, 9161–9175.

Esnouf, R. M. (1997). *J. Mol. Graph.* **15**, 132–134.

Fermi, G., Perutz, M. F., Shaanan, B. & Fourme, R. (1984). *J. Mol. Biol.* **175**, 159–174.

Geibel, J., Chang, C. K. & Traylor, T. G. (1975). *J. Am. Chem. Soc.* **97**, 5924–5926.

Gupta, R. K., Benovic, J. L. & Rose, Z. B. (1979). *J. Biol. Chem.* **254**, 8250–8255.

Janin, J. & Wodak, S. J. (1993). *Proteins*, **15**, 1–4.

Jayaraman, V. & Spiro, T. G. (1995). *Biochemistry*, **34**, 4511–4515.

Kaminaka, S. & Kitagawa, T. (1992). *J. Am. Chem. Soc.* **114**, 3256–3260.

Koshland, D. E. Jr, Némethy, G. & Filmer, D. (1966). *Biochemistry*, **5**, 365–385.

Lee, A. W., Karplus, M., Poyart, C. & Bursaux, E. (1988). *Biochemistry*, **27**, 1285–1301.

Lukin, J. A., Kontaxis, G., Simplaceanu, V., Yuan, Y., Bax, A. & Ho, C. (2003). *Proc. Natl Acad. Sci. USA*, **100**, 517–520.

Marden, M. C., Kister, J., Bohn, B. & Poyart, C. (1988). *Biochemistry*, **27**, 1659–1664.

Merritt, E. A. & Murphy, M. E. P. (1994). *Acta Cryst.* D**50**, 869–873.

Minton, A. P. & Imai, K. (1974). *Proc. Natl Acad. Sci. USA*, **71**, 1418–1421.

Monod, J., Wyman, J. & Changeux, J.-P. (1965). *J. Mol. Biol.* **12**, 88–118.

Mueser, T. M., Rogers, P. H. & Arnone, A. (2000). *Biochemistry*, **39**, 15353–15364.

Navaza, J. (1994). *Acta Cryst.* A**50**, 157–163.

Noble, R. W., Kwiatkowski, L. D., De Young, A., Davis, B. J., Haedrich, R. L., Tam, L. T. & Riggs, A. F. (1970). *Biochim. Biophys. Acta*, **870**, 552–563.

Perrella, M., Benazzi, L., Shea, M. A. & Ackers, G. K. (1990). *Biophys. Chem.* **35**, 97–103.

Perrella, M. & Di Cera, E. (1998). *J. Biol. Chem.* **274**, 2605–2608.

Perutz, M. F. (1970). *Nature (London)*, **228**, 726–734.

Perutz, M. F. (1972). *Nature (London)*, **237**, 459–499.

Perutz, M. F. (1989). *Q. Rev. Biophys.* **22**, 139–237.

Perutz, M. F., Wilkinson, A. J., Paoli, M. & Dodson, G. G. (1998). *Annu. Rev. Biophys. Biomol. Struct.* **27**, 1–34.

Safo, M. K., Abdulmalik, O., Danso-Danquah, R., Burnett, J. C., Nokuri, S., Joshi, G. S., Musayev, F. N., Asakura, T. & Abraham, D. J. (2004). *J. Med. Chem.* **47**, 4665–4676.

Safo, M. K. & Abraham, D. J. (2003). *Methods Mol. Med.* **82**, 1–19.

Safo, M. K. & Abraham, D. J. (2005). *Biochemistry*, **44**, 8347–8359.

Safo, M. K., Burnett, J. C., Musayev, F. N., Nokuri, S. & Abraham, D. J. (2002). *Acta Cryst.* D**58**, 2031–2037.

Sankaranarayanan, R., Biswal, B. K. & Vijayan, M. (2005). *Proteins*, **60**, 547–551.

Sawicki, C. A. & Gibson, Q. H. (1976). *J. Biol. Chem.* **251**, 1533–1542.

Schumacher, M. A., Zheleznova, E. E., Poundstone, K. S., Kluger, R., Jones, R. T. & Brennan, R. G. (1997). *Proc. Natl Acad. Sci. USA*, **94**, 7841–7844.

Schweitzer-Stenner, R., Wedekind, D. & Dreybrodt, W. (1986). *Biophys. J.* **49**, 1077–1088.

Silva, M. M., Rogers, P. H. & Arnone, A. (1992). *J. Biol. Chem.* **267**, 17248–17256**.**

Smith, F. R., Lattman, E. E. & Carter, C. W. Jr (1991). *Proteins*, **10**, 81–91.

Srinivasan, R. & Rose, G. D. (1994). *Proc. Natl Acad. Sci. USA*, **91**, 11113–11117.

Tian, W. D., Sage, J. T. & Champion, P. M. (1993). *J. Mol. Biol.* **233**, 155–166.

Traylor, T. G., Deardurff, L. A., Coletta, M., Ascenzi, P., Antonini, E. & Brunori, M. (1983). *J. Biol. Chem.* **258**, 12147–12148.

Vallone, B., Nienhaus, K., Matthes, A., Brunori, M. & Nienhaus, G. U. (2004). *Proc. Natl Acad. Sci. USA*, **101**, 17351–17356.

Vásquez, G. B., Ji, X., Fronticelli, C. & Gilliland, G. L. (1998). *Acta Cryst.* D**54**, 355–366.

Yang, F. & Phillips, G. N. Jr (1996). *J. Mol. Biol.* **256**, 762–774.

Yonetani, T., Parks, S., Tsuneshige, A., Imai, K. & Kanaori, K. (2002). *J. Biol. Chem.* **277**, 34508–34520.